

Article

# Silver-Sulfamethazine-Conjugated $\beta$ -Cyclodextrin/Dextran-Coated Magnetic Nanoparticles for Pathogen Inhibition

Anastasiia B. Shatan <sup>1,2</sup> , Vitalii Patsula <sup>1</sup>, Hana Macková <sup>1</sup>, Andrii Mahun <sup>1,2</sup>, Renáta Lehotská <sup>3</sup>, Elena Piecková <sup>3</sup> and Daniel Horák <sup>1,\*</sup> 

<sup>1</sup> Institute of Macromolecular Chemistry, Czech Academy of Sciences, Heyrovského nám. 2, 162 00 Prague 6, Czech Republic; shatan@imc.cas.cz (A.B.S.); patsula@imc.cas.cz (V.P.); mackova@imc.cas.cz (H.M.); mahun@imc.cas.cz (A.M.)

<sup>2</sup> Department of Physical and Macromolecular Chemistry, Faculty of Science, Charles University, Hlavova 8, 128 00 Prague 2, Czech Republic

<sup>3</sup> Institute of Microbiology, Faculty of Medicine, Slovak Medical University in Bratislava, Limbová 12, 83 303 Bratislava, Slovakia; renata.lehotska@szu.sk (R.L.); elena.pieckova@szu.sk (E.P.)

\* Correspondence: horak@imc.cas.cz

**Abstract:** In the fight against antibiotic resistance, which is rising to dangerously high levels worldwide, new strategies based on antibiotic-conjugated biocompatible polymers bound to magnetic nanoparticles that allow the drug to be manipulated and delivered to a specific target are being proposed. Here, we report the direct surface engineering of nontoxic iron oxide nanoparticles (IONs) using biocompatible dextran (Dex) covalently linked to  $\beta$ -cyclodextrin ( $\beta$ -CD) with the ability to form non-covalent complexes with silver-sulfamethazine (SMT-Ag). To achieve a good interaction of  $\beta$ -CD-modified dextran with the surface of the nanoparticles, it was functionalized with diphosphonic acid (DPA) that provides strong binding to Fe atoms. The synthesized polymers and nanoparticles were characterized by various methods, such as nuclear magnetic resonance (NMR), Fourier transform infrared (FTIR) and ultraviolet–visible (UV–Vis) spectroscopies, transmission electron microscopy (TEM), thermogravimetric analysis (TGA), atomic absorption spectroscopy (AAS), dynamic light scattering (DLS), etc. The resulting magnetic ION@DPA-Dex- $\beta$ -CD-SMT-Ag nanoparticles were colloidally stable in water and contained 24  $\mu$ g of antibiotic per mg of the particles. When tested for in vitro antimicrobial activity on Gram-positive (*Staphylococcus aureus*) and Gram-negative (*Escherichia coli*) bacteria and fungi (yeast *Candida albicans* and mold *Aspergillus niger*), the particles showed promising potential.

**Keywords:** superparamagnetic iron oxide nanoparticles;  $\beta$ -cyclodextrin; silver-sulfamethazine; antimicrobial activity



**Citation:** Shatan, A.B.; Patsula, V.; Macková, H.; Mahun, A.; Lehotská, R.; Piecková, E.; Horák, D. Silver-Sulfamethazine-Conjugated  $\beta$ -Cyclodextrin/Dextran-Coated Magnetic Nanoparticles for Pathogen Inhibition. *Nanomaterials* **2024**, *14*, 371. <https://doi.org/10.3390/nano14040371>

Academic Editor: Brigita Tomšič

Received: 7 February 2024

Revised: 14 February 2024

Accepted: 15 February 2024

Published: 17 February 2024



**Copyright:** © 2024 by the authors. Licensee MDPI, Basel, Switzerland. This article is an open access article distributed under the terms and conditions of the Creative Commons Attribution (CC BY) license (<https://creativecommons.org/licenses/by/4.0/>).

## 1. Introduction

Since the 1940s when antibiotics were first introduced to treat serious infections, they have achieved widespread use and saved millions of lives [1]. Among antibiotics, sulfonamides, such as sulfamethazine (SMT) derivatives, play an important role thanks to their broad spectrum of activity and low cost [2,3]. They are widely used in human medicine, as well as in animal production, to treat various bacterial infections of the soft tissues, urinary tract, lungs, ears and skin without noticeable toxicity to the tissues [4]. Their bacteriostatic activity is based on a competition with p-aminobenzoic acid, which is involved in the enzymatic synthesis of dihydrofolic acid. However, bacteria and other microorganisms have developed resistance to antibiotics, and this resistance is on the rise, prompting the need for new approaches using nanomedicine that can deliver antimicrobial agents precisely to a specific site, thereby minimizing their adverse effects [5].

A number of nanomaterials have been proposed for the delivery of biologically active agents to the required sites of action. In particular, superparamagnetic iron oxide nanopar-

ticles (IONs) have shown considerable potential [6]; for example, they have been used as anticancer or contrast agents in magnetic resonance imaging [7]. Their key advantage consists in magnetic field targeting, which allows high doses to be delivered, increasing the chances of successful treatment while reducing side effects. The functioning of IONs is dependent on many factors, such as shape, size, large surface-to-volume ratio, and the presence of reactive functional groups allowing the binding of various biological substances in sufficient quantities while maintaining colloidal stability. Colloidal stability in aqueous media is usually achieved by coating the IONs with various inorganic (silica) or synthetic organic polymers, such as poly(vinyl alcohol) and poly(ethylene glycol), as well as biopolymers like poly(L-lysine), dextran, chitosan, etc. [8]. Among these, dextran is the preferred choice for ION coating due to its biocompatibility, non-toxicity, degradability and the fact that it was FDA-approved for this purpose [9]. In addition, dextran is easily modifiable by tosylation, and various bioactive molecules can be bound by subsequent nucleophilic displacement reactions [10–12]. IONs have also been functionalized with  $\beta$ -cyclodextrin ( $\beta$ -CD), which belongs to a class of macrocycles consisting of seven glucose units, in order to remove pharmaceutical residues from water [13], remove cancer biomarkers from urine [14] or deliver hydrophobic drugs [15]. It is an advantage of  $\beta$ -CD that it is reactive towards biomolecules in aqueous media under mild conditions, preferably in combination with divinyl sulfone. For example,  $\beta$ -CD was found to form glutathione-responsive nanoparticles loaded with lonidamine for the simultaneous delivery of anticancer drugs into cancer cells [16] or to produce a complex based on silica-coated or imprinted IONs for the separation and recovery of erythromycin or doxycycline from industrial wastewater [17,18]. At the same time, the ability of  $\beta$ -CD as a host to form various supramolecular structures and to encapsulate guest molecules, e.g., sulfamethazine (SMT), by complexation in internal hydrophobic cavity was exploited, thus increasing the solubility and bioavailability of poorly soluble molecules [19]. However, it should be noted that SMT has rather limited biocidal activity; for example, the minimum inhibitory concentration (MIC) against *Escherichia coli* bacteria is 250  $\mu\text{g}/\text{mL}$ . In this respect, metal complexes of sulfonamides with higher antibacterial activity than free sulfamethazine are more promising, e.g., silver-sulfamethazine (SMT-Ag) has MIC = 100  $\mu\text{g}/\text{mL}$  [4]. In addition, silver is known to exhibit extensive biocidal effects, including antiviral and antifungal [20], for example in dentistry [21]. There are a number of methods to synthesize Ag nanoparticles, including laser ablation, irradiation, evaporation and condensation, lithography, microwave-assisted and green synthesis (from plants or microorganisms), polyol, photochemical and microemulsion methods and even electrodeposition [22].

The aim of this report was to design and synthesize new magnetic IONs coated with dextran and  $\beta$ -cyclodextrin as carriers of the SMT-Ag antibiotic for targeted pathogen inhibition. The *in vitro* antibacterial/antifungal activity of the newly synthesized nanoparticles was tested by standardized methods according to the European Committee on Antimicrobial Susceptibility Testing (EUCAST).

## 2. Experimental Procedures

### 2.1. Chemicals and Materials

$\text{FeCl}_2 \cdot 4\text{H}_2\text{O}$ ,  $\text{FeCl}_3 \cdot 6\text{H}_2\text{O}$ ,  $\beta$ -cyclodextrin ( $\beta$ -CD), sulfamethazine (SMT), divinyl sulfone (DVS), 4-toluenesulfonyl chloride (TsCl), 4-toluenesulfonic acid monohydrate (TsOH), ethanolamine (EA), lithium chloride and dextran ( $M_w = 70$  kDa) were purchased from Sigma-Aldrich (St. Louis, MO, USA). Hydrochloric acid (35%), sodium hydroxide, ammonium chloride, ethanol, acetone, hexane, dichloromethane (DCM) and other solvents were obtained from Lach-Ner (Neratovice, Czech Republic). Dimethylacetamide (DMAc) was purchased from Fluka (Buchs, Switzerland) and distilled before use. Vinylidene 1,1-diphosphonic acid (VDPA) was prepared as previously reported [23]. Silver-sulfamethazine (SMT-Ag) was prepared according to a previous publication [4]. Ultrapure Q-water filtered on a Milli-Q Gradient A10 system (Millipore; Molsheim, France) was used in the experiments.

Bacteria *Staphylococcus aureus* CCM 2022 and *Escherichia coli* CCM 3954 were obtained from the collection of pathogenic microorganisms at the Slovak Medical University (SMU) in Bratislava, Slovakia. Ascomycetous fungi *Candida albicans* (CCM 8186; CA) and *Aspergillus niger* (AN; environmental isolate from the fungal collection) were from the Mycological laboratory of SMU.

## 2.2. Synthesis of 4-Toluenesulfonic Anhydride (Ts<sub>2</sub>O) and 6-Toluenesulfonyl-β-Cyclodextrin (β-CD-Ts)

Ts<sub>2</sub>O was prepared by modification of the previous procedure [24]. Briefly, a solution of TsCl (8 g; 42 mol) and TsOH H<sub>2</sub>O (2 g; 11 mol) in DCM (50 mL) was stirred (600 rpm) at room temperature (RT) for 16 h and filtered through silica gel. After drying under vacuum (133 Pa), 5.8 g of Ts<sub>2</sub>O (73% yield) was obtained; its structure was confirmed by <sup>1</sup>H NMR spectroscopy by comparison with TsCl and TsOH (Supplementary Material; Figure S1).

A suspension of β-CD (5.75 g; 5 mmol; <sup>1</sup>H NMR spectrum is shown in Figure S2a) and Ts<sub>2</sub>O (3.3 g; 10 mmol) in water (125 mL) was stirred at RT for 2 h, an aqueous 0.125 M NaOH solution (25 mL) was added, and, after 10 min, unreacted Ts<sub>2</sub>O was removed by filtration through a nylon membrane filter (0.2 μm pores). NH<sub>4</sub>Cl (6.7 g) was added to the filtrate, and its pH was adjusted to ~8. The resulting β-CD-Ts solution was cooled to 4 °C for 16 h, the precipitate was separated and washed with cold water and acetone. After drying under vacuum (133 Pa), a white β-CD-Ts powder was obtained; the structure of β-CD-Ts was confirmed by <sup>1</sup>H NMR (Figure S2b).

## 2.3. Synthesis of 6-Deoxy-6-Hydroxyethylamino-β-Cyclodextrin (β-CD-EA) and 6-Deoxy-6-(2-Hydroxyethyl) (Vinylsulfonyl)Methylamino-β-Cyclodextrin (β-CD-VS)

β-CD-EA and β-CD-VS were also prepared by modifying the earlier procedure [25]. AE (2.72 mL; 45 mmol) was added to a solution of β-CD-Ts (1.16 g; 0.9 mmol) in dimethylformamide (DMF; 10 mL), and the reaction mixture was stirred (600 rpm) at 80 °C for 48 h. Tetrahydrofuran (THF; 100 mL) was then added, and the resulting β-CD-EA precipitate was filtered, washed with THF (30 mL) and dried under vacuum (133 Pa); the structure of β-CD-EA was demonstrated by <sup>1</sup>H NMR and DOSY spectra (Figure S3a,c).

To a solution of β-CD-EA (1 g; 0.83 mmol) in water (8 mL) was added divinyl sulfone (0.2 mL; 2.07 mmol), and the reaction mixture was maintained at RT for 2 h. Next, THF (80 mL) was added, and the resulting β-CD-VS precipitate was filtered off, washed with THF (10 mL) and dried in vacuum; the structure of β-CD-VS was confirmed by <sup>1</sup>H NMR and DOSY spectra (Figure S3b,d).

## 2.4. Tosylation of Dextran and the Reaction of Dex-Ts with Ethanolamine (EA)

6-Toluenesulfonyl dextran (Dex-Ts) was prepared by modifying an earlier procedure [12]. Briefly, dextran (5 g) and anhydrous LiCl (3.0 g; 70.8 mmol) were dissolved in DMAc (125 mL) at 80 °C with stirring (600 rpm). Next, a solution of triethylamine (25.78 mL; 184.8 mmol) in DMAc (24 mL) and a solution of TsCl (17.62 g; 92.4 mmol) in DMAc (24 mL) were added dropwise at 8 °C; the mixture was allowed to react for 36 h with stirring (400 rpm). Dex-Ts was isolated by double precipitation in water (600 mL) and dried at RT under vacuum (133 Pa). The structure of Dex-Ts was proven by <sup>1</sup>H NMR (Figure S4a).

To a solution of Dex-Ts (3 g) in DMF (30 mL) was added EA (23.95 mL; 396 mmol), and the reaction mixture was stirred (600 rpm) at 90 °C for 48 h. 6-Deoxy-6-hydroxyethylaminodextran (Dex-EA) was isolated by double precipitation in THF (100 mL), purified on a Sephadex<sup>®</sup> G-25 column and lyophilized; the structure of Dex-EA was proven by <sup>1</sup>H NMR (Figure S4b).

## 2.5. Functionalization of Dex-EA with β-CD-VS and Modification with VDPA

First, Dex-β-CD was obtained by reacting an aqueous solution (10 mL) of Dex-EA (0.25 g; 1.19 mmol) with an aqueous solution (15 mL) of β-CD-VS (0.78 g; 0.6 mmol) under stirring at 37 °C for 24 h. Dex-β-CD was then dialyzed (MWCO = 12–14 kDa) against water for 72 h and lyophilized. Subsequently, an aqueous solution (1 mL) of VDPA (0.07 g;

0.38 mmol), whose pH was adjusted to 10.8 with 10 M NaOH, was added to an aqueous solution (8 mL) of Dex- $\beta$ -CD (0.25 g), and the mixture was stirred (800 rpm) at 50 °C for 24 h. The resulting 1,1-diphosphonic acid-terminated  $\beta$ -cyclodextrin/dextran (DPA-Dex- $\beta$ -CD) conjugate was purified on a Sefadex G-25 column with water as eluent; the pH was adjusted to 2 by the addition of 1 M HCl, purified once more and lyophilized. The successful functionalization of Dex-EA with  $\beta$ -CD-VS and modification with VDPA was confirmed by  $^1\text{H}$  NMR (Figure S5a),  $^{13}\text{C}$  NMR (Figures S5b and S6) and  $^{13}\text{C}$  NMR spectra (Figure S7).

#### 2.6. Synthesis of Iron Oxide Nanoparticles (IONs)

The iron oxide dispersion was prepared according to a previously published coprecipitation method [26]. Briefly, an aqueous solution of 0.2 M iron(III) chloride (100 mL) and 0.2 M iron(II) chloride (50 mL) was sonicated with 0.5 M aqueous  $\text{NH}_4\text{OH}$  (100 mL) for 5 min. The solution was then added to a 0.5 M aqueous  $\text{NH}_4\text{OH}$  solution (400 mL) and stirred (200 rpm) at RT for 1 h. Afterward, the resulting precipitate was separated using a magnet and washed repeatedly with water until peptization, during which colloidal nanoparticles were formed. Subsequently, the particles were sonicated with a 5 wt.% sodium hypochlorite solution (16 mL) for 5 min, and the resulting IONs were separated and washed as described above to a concentration of 42 mg per mL.

#### 2.7. Complexation of ION@DPA-Dex- $\beta$ -CD Nanoparticles with Silver-Sulfamethazine (SMT-Ag)

ION@DPA-Dex- $\beta$ -CD particles were prepared by mixing an aqueous solution (4 mL) of DPA-Dex- $\beta$ -CD conjugate (40 mg) with an aqueous dispersion of IONs (6 mL; 40 mg particles) under sonication, followed by stirring (800 rpm) at RT for 3 days. The resulting ION@DPA-Dex- $\beta$ -CD particles were magnetically separated and washed with water three times (10 mL each) using centrifugation. The mixture of SMT-Ag (10 mg) in 0.06%  $\text{NH}_4\text{OH}$  (10 mL) was sonicated for 5 min and added; the whole mixture was stirred (800 rpm) at RT for 3 days, and the resulting ION@DPA-Dex- $\beta$ -CD-SMT-Ag particles were washed as described above. IONs, ION@DPA-Dex- $\beta$ -CD and ION@DPA-Dex- $\beta$ -CD-SMT-Ag particles used in biological experiments were ultrasonically sterilized (Bandelin Sonopuls; Berlin, Germany; 20% power) for 2 min and diluted with aqua pro injection to 4 mg/mL in an MSC-Advantage biological safety cabinet (Thermo Fisher Scientific; Waltham, MA, USA).

To determine the SMT-Ag content in the nanoparticles, an aqueous dispersion (0.9 mL) of ION@DPA-Dex- $\beta$ -CD-SMT-Ag particles (1 mg) was dissolved in 38% aqueous hydrofluoric acid (0.1 mL) with shaking for 30 min, the precipitated Ag was removed by centrifugation (14,100 rcf) for 20 min, the solution was optionally diluted with water and the absorbance was measured at 300 nm using an Evolution™ 220 UV-Vis spectrometer (Thermo Fisher Scientific; Waltham, MA USA); the absorbance was then compared with the calibration curve of a solution of pure SMT in 2% aqueous hydrofluoric acid. The reference sample was prepared as described above but with particles without SMT-Ag. The SMT-Ag loading efficiency (LE) was determined from the SMT-Ag content according to the following equation:

$$LE (\%) = m_{\text{SMT encap}} / m_{\text{carrier total}} \times 100 \quad (1)$$

where  $m_{\text{SMT encap}}$  is the mass of SMT-Ag in particles and  $m_{\text{carrier total}}$  is the mass of ION@DPA-Dex- $\beta$ -CD-SMT-Ag.

The solubility of SMT-Ag with or without  $\beta$ -CD in 0.06%  $\text{NH}_4\text{OH}$  was determined by UV-Vis spectroscopy. SMT-Ag (20 mg), optionally with  $\beta$ -CD (56 mg), was added to 0.06%  $\text{NH}_4\text{OH}$  (10 mL), and the mixture was sonicated for 3 min. The resulting dispersion was stirred vigorously at RT for 2 days, then centrifuged (6850 rcf) for 60 min and filtered through a 0.45  $\mu\text{m}$  filter. The solution (0.9 mL) was mixed with 38% aqueous hydrofluoric acid solution (0.1 mL), diluted five times with water, and the absorbance was measured at 300 nm. The amount of dissolved antibiotic was determined from the SMT calibration curve in 2% aqueous hydrofluoric acid.

### 2.8. Physicochemical Characterization of Particles and Their Coatings

Transmission electron micrographs were taken on a Tecnai Spirit G2 transmission electron microscope (TEM; FEI; Brno, Czech Republic) at 120 kV to determine the number-average diameter ( $D_n = \sum N_i \cdot D_i / \sum N_i$ ), weight-average diameter ( $D_w = \sum N_i \cdot D_i^4 / \sum N_i \cdot D_i^3$ ) and dispersity ( $D = D_w / D_n$ ) from at least 300 particles using Atlas software (Tescan Digital Microscopy Imaging; Brno, Czech Republic). Dynamic light scattering (DLS) was measured on a Zetasizer Ultra analyzer (Malvern Panalytical; Malvern, UK) to determine the hydrodynamic diameter ( $D_h$ ), polydispersity ( $PD$ ) and  $\zeta$ -potential of the nanoparticles in water (pH = 5.6).

$^1\text{H}$ ,  $^{13}\text{C}$  and  $^{31}\text{P}$  NMR spectra were recorded using a Bruker Avance III 600 spectrometer at Larmor frequencies of  $\nu(^1\text{H}) = 600.2$  MHz,  $\nu(^{13}\text{C}) = 150.9$  MHz and  $\nu(^{31}\text{P}) = 242.9$  MHz, respectively, and processed with Bruker TopSpin 4.1.1 software. The samples were dissolved either in DMSO- $d_6$  or  $\text{D}_2\text{O}$  at 22 °C.  $^1\text{H}$  NMR spectra were obtained using a 90° pulse (18  $\mu\text{s}$  length) with a 10 s recycle delay and 16–64 number of scans.  $^1\text{H}$ - $^1\text{H}$  2D nuclear Overhauser effect NMR spectra (NOESY) were recorded with a spectral window of 7200 Hz in both F1 and F2 frequency dimensions and with a mixing time of 500 ms. A total of 32 scans were accumulated over 512  $t_1$  increments with a relaxation delay of 10 s. The diffusion of the components in the samples was investigated by pulsed-field gradient NMR using a 2D diffusion-ordered spectroscopy (DOSY) with a DiffBB diffusion probehead and 40 A gradient amplifiers. A double-stimulated echo pulse sequence was used to measure the self-diffusion coefficients  $D$  obtained by least-squares fitting of the Stejskal–Tanner equation [27] using Bruker Dynamics center 2.6.1 software. Experiments were performed with a diffusion time of 50 ms, a gradient duration of 1 ms and a gradient strength varying in 8 steps with a maximum of 2 T/m.  $^{13}\text{C}$  NMR spectra were recorded using a 90° pulse (10  $\mu\text{s}$  length) with a 10 s recycle delay and 5–20 k number of scans.  $^{31}\text{P}$  NMR spectra were obtained using a 90° excitatory pulse (18  $\mu\text{s}$  length) with a 10 s recycle delay and 1024 scans. In the case of  $^{13}\text{C}$  and  $^{31}\text{P}$  NMR spectra, inverse-gated decoupling was used to remove heteronuclear interactions.  $^1\text{H}$  and  $^{13}\text{C}$  chemical shifts were calibrated using hexamethyldisiloxane (0.05 ppm from tetramethylsilane in  $^1\text{H}$  NMR spectra and 2 ppm in  $^{13}\text{C}$  NMR spectra) as an external standard.  $^{31}\text{P}$  NMR chemical shift was calibrated using  $\text{H}_3\text{PO}_4$  in  $\text{D}_2\text{O}$  (0 ppm) as an external standard.

FTIR spectra were acquired on a Perkin-Elmer Paragon 1000PC spectrometer (Waltham, MA, USA) using a Specac MKII Golden Gate single attenuated total reflection (ATR) system with a diamond crystal and a 45° angle of incidence.

The C, H, N and S contents in the polymers were determined using a FlashSmart™ elemental analyzer (Thermo Fisher Scientific; Waltham, MA, USA). The phosphorus content in the polymer was determined after its digestion in a  $\text{HClO}_4/\text{HNO}_3$  mixture in a Biotage Initiator microwave reactor (Biotage AB; Uppsala, Sweden) in the presence of sulfuric acid, ammonium molybdate, ascorbic acid and potassium antimony tartrate. Spectra were recorded on a Libra S22 UV–Vis spectrophotometer (Biochrom; Cambridge, UK) at 690 nm; calibration with  $\text{KH}_2\text{PO}_4$ .

### 2.9. Disc Diffusion Test (DDT) for Qualitative Antibimicrobial Evaluation

Briefly, sterile filter paper discs (5 or 10 mm diameter; Whatmann, Bio-Rad; Hercules, CA USA) were loaded with stock dispersions of IONs, ION@DPA-Dex- $\beta$ -CD and ION@DPA-Dex- $\beta$ -CD-SMT-Ag particles (10 or 30  $\mu\text{L}$ ; 4 mg/mL) to achieve the desired concentration per disc (40 or 120  $\mu\text{g}$ ) and dried at RT. Pure colonies of Gram-positive *S. aureus* and Gram-negative *E. coli* strains isolated from fresh growth were transferred into sterile saline and vortexed to form a homogeneous bacterial suspension according to the protocol recommended by EUCAST [28]. The optical density (OD) was then adjusted to a 0.5 McFarland standard and used as an inoculum suspension.

The same protocol was used for *C. albicans* as for bacterial strains. A 24 h yeast culture was transferred into sterile saline and vortexed to form a homogeneous suspension. The OD of suspension was then adjusted to 0.5 McFarland, and the suspension was diluted

with sterile saline 1:10 *v/v* and used as a standardized inoculum. For the fungal strain, a modified protocol described previously was followed [29].

*A. niger* was subcultured on a Sabouraud dextrose agar plate (HiMedia; Mumbai, India) at 37 °C for 7 days. After culture growth, conidia were harvested in a sterile saline solution with 0.1% Tween 80. The purity of the conidial suspension was checked under a microscope to ensure that no hyphae were present and then adjusted to OD = 0.5 McFarland. Another conidial suspension was diluted 1:10 *v/v* with sterile saline with 0.1% Tween 80 and used as a standardized inoculum suspension.

Standardized inoculum suspensions were swabbed evenly over Mueller–Hinton agar (MHA) plates (Oxoid; Basingstoke, UK). The prepared discs were fixed in triplicates on the surface of the inoculated agar plate within 15 min of inoculation. In the case of ION@DPA-Dex-β-CD-SMT-Ag, a 10 μL drop of undiluted solution was dropped onto the plate with each tested microorganism. Finally, inhibition zone diameters (mm) and growth in the droplet were checked after static incubation at 37 °C for 24 h for bacteria and candida or up to 72 h for *A. niger*.

### 2.10. Minimum Inhibitory and Minimum Bactericidal/Microbicidal Concentrations (MIC and MBC/MMC)

According to EUCAST recommendations, the international ISO 20776-1 standard was followed. A quantitative microdilution broth assay was used to investigate antimicrobial susceptibility against *S. aureus* for all three test substances—IONs, ION@DPA-Dex-β-CD and ION@DPA-Dex-β-CD-SMT-Ag. The MIC of ION@DPA-Dex-β-CD-SMT-Ag was also tested with *E. coli*, *C. albicans* and *A. niger*. Briefly, 96 flat-bottom microtiter plates for tissue cultures were used, and the tests were performed in parallel. A set of particle concentrations of 1500–2.5 μg/mL (1500, 1000, 500, 250, 125, 50, 25, 12.5, 5 and 2.5 μg/mL) was prepared by diluting the stock solution with Mueller–Hinton broth (Oxoid) and pipetted into the respective wells. Positive control (growth) consisted of culture solution in the absence of an antimicrobial agent and with microbial inoculum. Negative control (growth) consisted of dilution solutions without culture broth in the presence of microbial inoculum. After inoculation with the standardized suspension of the microorganism, the plates were incubated at 37 °C for 18 h. The microbial growth on the plates was evaluated by the naked eye, and the lowest concentration of antimicrobial agent expressed in μg/mL, which visibly inhibited the growth of the microorganism in both parallel experiments, was recorded as MIC. The viability of the inoculum was checked according to the method used.

After MIC determination, MBC/MMC was evaluated according to the following procedure. For each concentration from the MIC test for which no growth was observed in the parallel wells, 10 μL of the solution from both wells was inoculated onto MHA plates and incubated at 37 °C for an additional 24 h. If no growth was observed in both parallel drops, the corresponding concentration was read as MBC/MMC.

## 3. Results and Discussion

### 3.1. Iron Oxide Nanoparticles (IONs)

The IONs were synthesized by the precipitation of iron(II) and (III) chlorides with ammonium hydroxide, which is a frequently used method for the preparation of magnetic nanoparticles [26,30]. It is supposed that the resulting product consisted predominantly of magnetite, which is not very stable and may undergo uncontrolled oxidation to other forms of iron oxide, including non-magnetic hematite. In order to prevent the uncontrolled oxidation of magnetite, its controlled oxidation to maghemite using sodium hypochlorite was carried out. Such IONs have the advantage of superparamagnetism, which means that they respond to an external magnetic field but do not retain residual magnetism when the magnetic field is removed, and therefore do not agglomerate and are readily dispersible in aqueous media [31]. Superparamagnetism of IONs is then advantageously used in many biomedical applications [32]. The morphology of IONs in a dry state was investigated by TEM (Figure 1), which revealed particle aggregates formed during sample preparation

involving drop casting and drying. The aggregates consisted of primary particles with a shape close to spherical, with an average size of  $D_n = 8 \pm 2$  nm and dispersity  $D = 1.29$ , indicating a moderately broad size distribution. In addition to TEM analysis of the dry particles, the aqueous dispersion of IONs was investigated by DLS, which revealed a hydrodynamic diameter  $D_h = 108 \pm 1$  nm and a polydispersity  $PD = 0.13$ . A larger  $D_h$  than  $D_n$  is common for ION colloids not only because of partial aggregation but also because the particles are surrounded by an electrical double layer and DLS measures an intensity-weighted z-average diameter sensitive to large objects. DLS is also used to measure the  $\xi$ -potential, which reached  $-26 \pm 5$  mV; the negative  $\xi$ -potential is typical for particles prepared by coprecipitation of  $\text{FeCl}_2$  and  $\text{FeCl}_3$  with a base [33]. Such a value of the  $\xi$ -potential ensures the colloidal stability of the IONs in water [34]. According to the TGA of neat IONs, 3.1 wt.% of the total weight loss could be attributed to the evaporation of residual water.

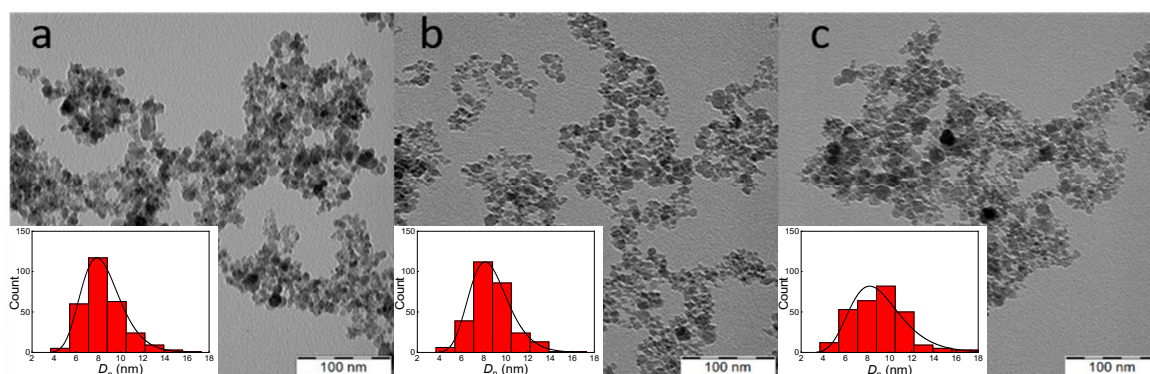


**Figure 1.** TEM micrographs of (a) IONs, (b) ION@DPA-Dex- $\beta$ -CD and (c) ION@DPA-Dex- $\beta$ -CD-SMT-Ag particles.

### 3.2. Modification of Dex and $\beta$ -CD

Because SMT-Ag has limited solubility in water, it cannot be directly used *in vivo*, and it is necessary to incorporate it into a hydrophilic carrier suitable for bioapplications.  $\beta$ -CD was chosen as the carrier of SMT-Ag in this work because it has a hydrophobic pocket into which the SMT can be easily loaded. The disadvantage of this system, however, is its low molar mass and therefore possible rapid renal clearance combined with non-specific targeting. Therefore,  $\beta$ -CD was bound to hydrophilic Dex containing diphosphonate anchoring groups capable of complexation with IONs. Dex is a biocompatible, biodegradable, non-toxic and non-immunogenic polymer [35], making it a promising platform for the design of biosafe particles that are colloiddally stable in water and body fluids.

The synthesis of a reactive  $\beta$ -CD derivative, 6-deoxy-6-(2-hydroxyethyl) (vinylsulfonyl) methylamino- $\beta$ -cyclodextrin ( $\beta$ -CD-VS), proceeded by a three-step process consisting of (i) tosylation of  $\beta$ -CD with *p*-toluenesulfonic anhydride ( $\text{Ts}_2\text{O}$ ) in water followed by treatment with 10% aqueous NaOH solution; (ii) the reaction of 6-*O*-monotosyl- $\beta$ -cyclodextrin ( $\beta$ -CD-Ts) with EA (1/50 mol/mol) in DMF to form mono-6-(2-hydroxyethyl)amino- $\beta$ -cyclodextrin ( $\beta$ -CD-EA) and (iii) the introduction of reactive vinyl groups by an aza-Michael reaction with DVS to form  $\beta$ -CD-VS (Figure 2). Simultaneously, the reaction of Dex with  $\text{TsCl}$  formed Dex-Ts, whose Ts groups were subsequently exchanged with ethanolamine to form Dex-EA, which was then reacted with the double bond of  $\beta$ -CD-VS, resulting in Dex- $\beta$ -CD (Figure 3). Dex- $\beta$ -CD finally reacted with VDPA to form DPA-Dex- $\beta$ -CD.

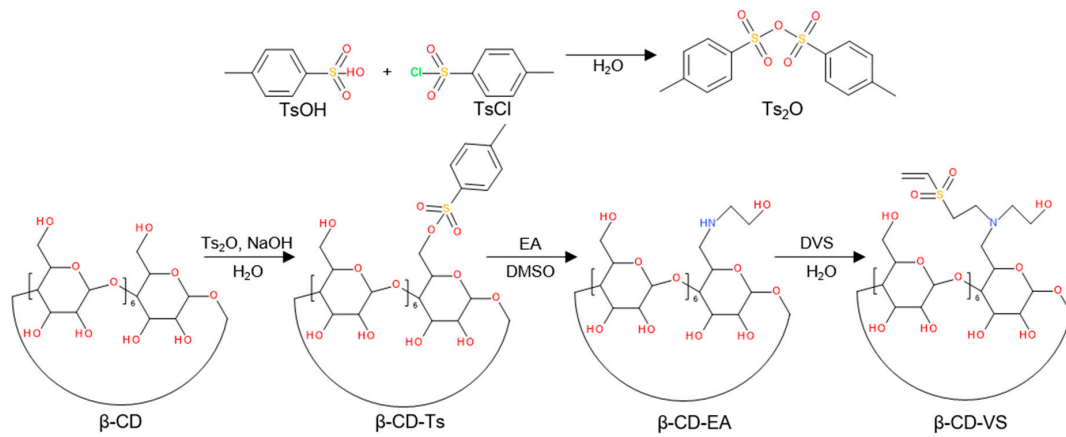


**Figure 2.** Synthesis of 4-toluenesulfonic anhydride (Ts<sub>2</sub>O) and three-step modification of β-cyclodextrin (β-CD) to yield 6-deoxy-6-(2-hydroxyethyl) (vinylsulfonyl)methylamino-β-cyclodextrin (β-CD-VS); EA—ethanolamine, DMSO—dimethyl sulfoxide, DVS—divinyl sulfone.

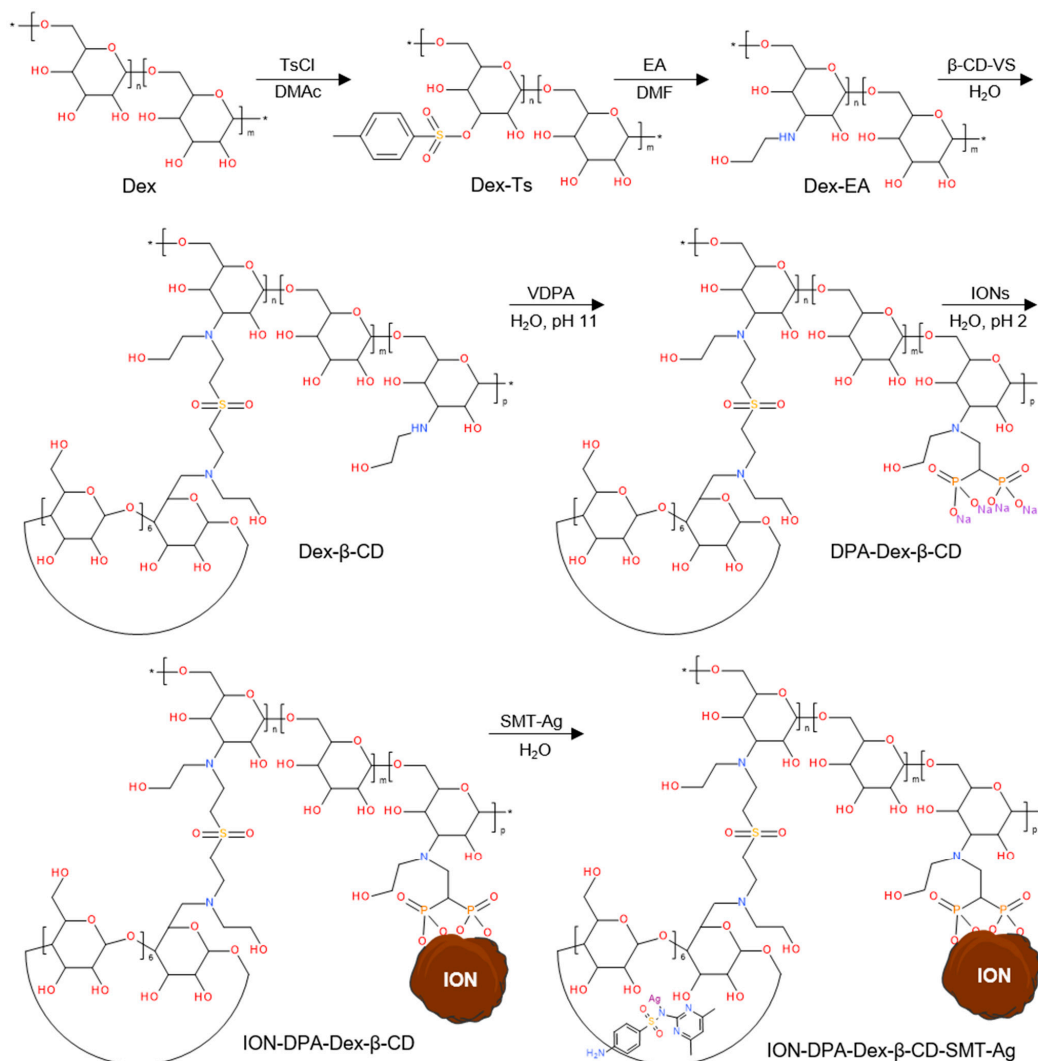


**Figure 3.** Modification of dextran with tosyl chloride (TsCl), ethanolamine (EA), 6-deoxy-6-(2-hydroxyethyl) (vinylsulfonyl)methylamino-β-cyclodextrin (β-CD-VS) and vinylidene 1,1-diphosphonic acid (VDPA) and conjugation of silver-sulfamethazine (SMT-Ag) to form silver-sulfamethazine-conjugated β-cyclodextrin/dextran-coated iron oxide nanoparticle (ION); DMAC—dimethylacetamide.

The structure of the individual components was confirmed by  $^1\text{H}$ ,  $^{13}\text{C}$  and  $^{31}\text{P}$  NMR spectra. For example, the  $^1\text{H}$  NMR spectrum of Dex-Ts displayed signals corresponding to the  $\alpha$ -1,6 glucose units of Dex, as well as signals of the tosyl groups bound to the Dex chains (Figure S4a). By comparing the integral signal intensity from the C1 proton of Dex with the signals from the aromatic protons of the tosyl groups, it was found that, on average, 72% of the glucose subunits of Dex have one -OH group substituted by a tosyl group. In addition, the structure of the Dex-EA was analyzed from the respective  $^1\text{H}$  and  $^{13}\text{C}$  NMR spectra (Figures S4b and S8). The almost complete substitution of Ts groups by EA was confirmed by a considerable decrease of NMR signals corresponding to Ts; only relatively small signals indicated residual Ts ( $\sim 7\%$  of glucose subunits of Dex still had adjacent Ts groups). In turn, signals from EA were clearly visible in the corresponding  $^{13}\text{C}$  NMR spectrum (Figure S8; signals marked as "7" and "8"); based on the relative intensity of these signals,  $\sim 65\%$  of glucose units in Dex were modified with EA. In the case of the  $^1\text{H}$  NMR spectrum of  $\beta$ -CD, its structure was confirmed by signals typical of glucose subunits linked by  $\alpha$ -1,4 glycosidic bonds (Figure S2a), which was in agreement with the literature [36]. The modification of  $\beta$ -CD by  $\text{Ts}_2\text{O}$  was confirmed by the presence of NMR signals corresponding to methyl and aromatic protons from Ts marked as "9", "8" and "7" (Figure S2b). In addition, the signals corresponding to the  $\beta$ -CD rings were broadened, which can be attributed to the change in  $\beta$ -CD solubility. Comparison of the integral NMR signal intensities from the C1 proton with those from Ts showed that, on average, one hydroxyl group of the  $\beta$ -CD ring was substituted by tosyl. To additionally confirm the chemical binding of Ts to  $\beta$ -CD, 2D NOESY and DOSY NMR spectra were recorded (Figure S2c,d). The NOESY spectrum showed cross-peaks (highlighted by the grey boxes in Figure S2d), indicating the close spatial proximity of the Ts groups and the  $\beta$ -CD rings and thus their chemical binding. In addition, diffusion NMR measurements revealed that both parts of the  $\beta$ -CD-Ts had similar values of the self-diffusion coefficient ( $D = \sim 1 \times 10^{-10} \text{ m}^2/\text{s}$ ), further confirming that they are chemically bound (Figure S2c).

Furthermore, the substitution of Ts groups of  $\beta$ -CD-Ts by EA was confirmed in the same way as in the case of Dex, i.e., from  $^1\text{H}$  and  $^{13}\text{C}$  NMR spectra (Figures S3a and S9). Nevertheless, low-intensity peaks corresponding to the Ts group were still present in the  $^1\text{H}$  NMR spectrum of  $\beta$ -CD-EA. Therefore, diffusion NMR spectra (2D DOSY) were recorded to determine whether these Ts groups were chemically bound to the  $\beta$ -CD rings. Since the self-diffusion coefficient of Ts moieties ( $3.27 \times 10^{-10} \text{ m}^2/\text{s}$ ) was much higher than that of  $\beta$ -CD-EA ( $1.03 \times 10^{-10} \text{ m}^2/\text{s}$ ), these groups attributed to the unwashed residual EA salt of  $\text{TsOH}$  were not bound to  $\beta$ -CD rings (Figure S3c). The introduction of vinyl groups by the reaction of  $\beta$ -CD-EA with DVS was confirmed by the presence of signals from vinyl protons marked as "9" and "10" in the  $^1\text{H}$  NMR spectrum of  $\beta$ -CD-VS (Figure S3b). Moreover, diffusion NMR measurements showed the same self-diffusion coefficient of the VS group as that of the  $\beta$ -CD ring ( $1.01 \times 10^{-10} \text{ m}^2/\text{s}$ ), indicating that VS was chemically bound to  $\beta$ -CD (Figure S3d).

In the case of DPA-Dex- $\beta$ -CD, the analysis and accurate peak assignment of the NMR signals in the  $^1\text{H}$  and  $^{13}\text{C}$  spectra were rather complicated because the subunits in modified Dex and  $\beta$ -CD have similar structures and therefore provide overlapping NMR signals (Figure S5). However, the formation of DPA-Dex- $\beta$ -CD by the reaction of the  $\beta$ -CD-VS double bond with Dex-EA could be deduced from the absence of NMR signals of the VS groups (Figure S5a). Moreover, in the  $^{13}\text{C}$  NMR spectrum of DPA-Dex- $\beta$ -CD, C1 carbon signals from both the Dex and  $\beta$ -CD subunits were distinguished, again suggesting that  $\beta$ -CD was bound with Dex (Figure S5c). In addition, by comparing the integral C1 signal intensity of the  $\beta$ -CD carbon rings at 102.58 ppm with the C1 signals of the Dex main chain and terminal groups at 98.77 and 101.17 ppm, respectively, the number of  $\beta$ -CD units in DPA-Dex- $\beta$ -CD was evaluated (Figure S6); on average,  $\sim 63\%$  of glucose units in Dex bound  $\beta$ -CD. Finally, the  $^{31}\text{P}$  NMR spectrum of DPA-Dex- $\beta$ -CD showed one main signal at 11.2 ppm corresponding to the diphosphonic acid groups (Figure S7).

Another technique to characterize both Dex and  $\beta$ -CD and their derivatives was FTIR spectroscopy (Figure 4a–c). The spectra of Dex and  $\beta$ -CD showed considerable similarity; the band at  $3300\text{--}3330\text{ cm}^{-1}$  was attributed to the hydroxyl stretching vibration ( $\nu_{\text{OH}}$ ) of the polysaccharide [37]. The band at  $2920\text{ cm}^{-1}$  was ascribed to the C–H stretching vibration, while the peak at  $912\text{ cm}^{-1}$  was due to the  $\alpha$ -glycosidic bond of Dex. Other major characteristic bands at  $1154$ ,  $1101$  and  $1010\text{ cm}^{-1}$  were ascribed to valence vibrations of C–O and C–C bonds and deformation vibrations of the CCH, COH and HCO bonds. The FTIR spectrum of the Dex-Ts showed typical Dex peaks and intense peaks at  $1175\text{ cm}^{-1}$  ( $\nu_{\text{sym}}\text{SO}_2$ ) and  $815\text{ cm}^{-1}$  ( $\delta\text{C-H}_{\text{ar}}$ ) characteristic of the tosyl [12]. The spectrum of  $\beta$ -CD-Ts showed similar bands at  $1360$ ,  $1175$  and  $813\text{ cm}^{-1}$  attributed to  $\nu_{\text{as}}$ ,  $\nu_{\text{sym}}\text{SO}_2$  stretching and  $\delta\text{C-H}_{\text{ar}}$  rocking vibrations, respectively. In the spectra of  $\beta$ -CD-EA and Dex-EA, the peak at  $1175\text{ cm}^{-1}$  assigned to the  $\nu_{\text{sym}}\text{SO}_2$  vibration disappeared, confirming the replacement of the tosyl group by ethanolamine. In contrast to  $\beta$ -CD-EA, the intensity of the peak at  $1300\text{ cm}^{-1}$  in the spectrum of  $\beta$ -CD-VS increased, which probably belonged to the  $\nu\text{SO}_2$  stretching vibration due to the functionalization of  $\beta$ -CD by the vinyl sulfone group [38]. In the spectrum of DPA-Dex- $\beta$ -CD, a new peak appeared at  $887\text{ cm}^{-1}$ , most probably assigned to the  $\nu\text{P-OH}$  vibration, confirming the introduction of diphosphonic acid groups into the polymer [39].

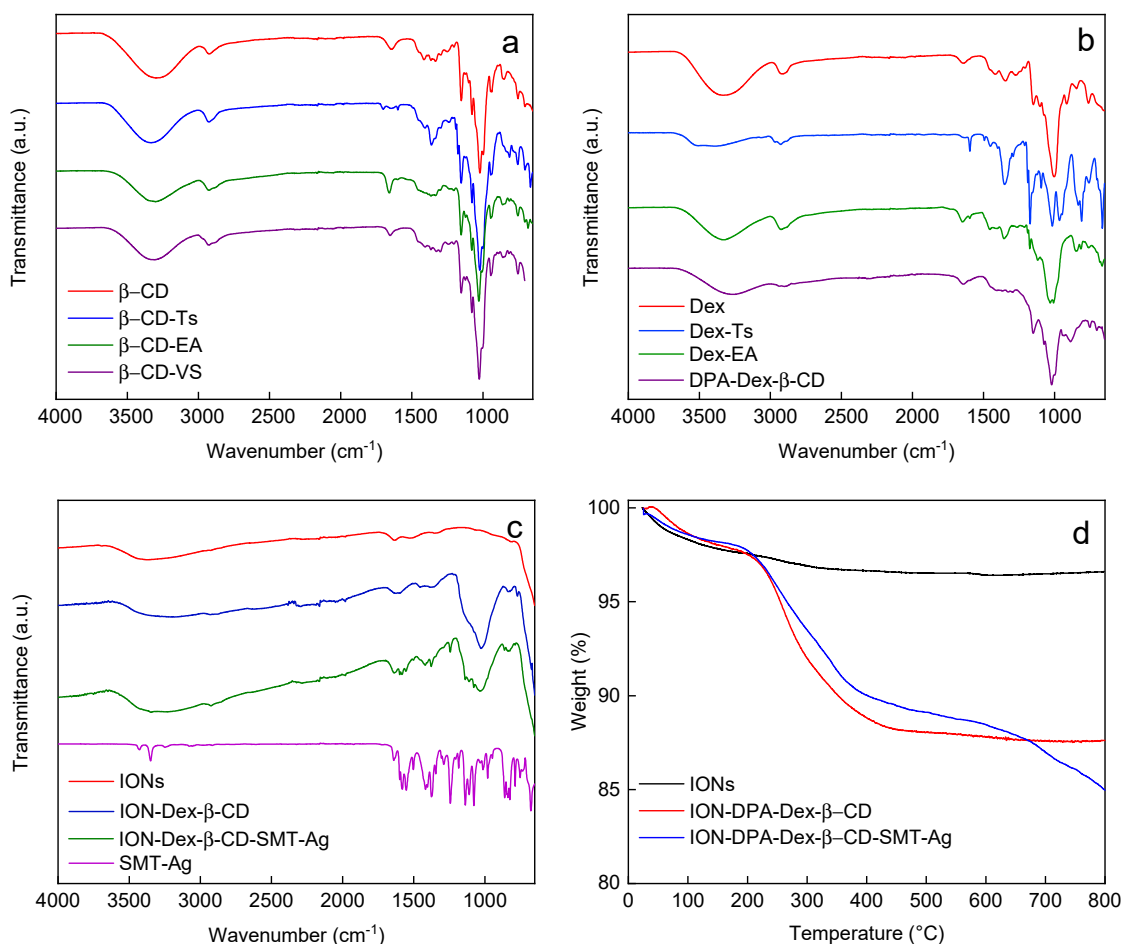


**Figure 4.** (a–c) FTIR and (d) TGA analysis of IONs,  $\beta$ -CD,  $\beta$ -CD-Ts,  $\beta$ -CD-EA,  $\beta$ -CD-VS, Dex, Dex-Ts, Dex-EA, SMT, DPA-Dex- $\beta$ -CD, ION-DPA-Dex- $\beta$ -CD and ION-DPA-Dex- $\beta$ -CD-SMT.

In addition, the successful reactions of Dex-EA with  $\beta$ -CD-VS and Dex- $\beta$ -CD with VDPA were confirmed by analysis of sulfur, phosphorus and nitrogen in both the starting  $\beta$ -CD and Dex derivatives and the final DPA-Dex- $\beta$ -CD conjugate (Table S1). While  $\beta$ -CD-Ts contained 2.33 wt.% sulfur, i.e., 93% of  $\beta$ -CD molecules were monotosylated,  $\beta$ -CD-EA

had 1.2 wt.% nitrogen, indicating full substitution of Ts groups. As  $\beta$ -CD-VS contained 2.04 wt.% sulfur, 82% of  $\beta$ -CD was modified with DVS. In the case of Dex-Ts containing 10.07 wt.% sulfur, all glucose units were assumed to be tosylated (Table S1), which was ~30% more than according to the  $^1\text{H}$  NMR spectrum. This may be due to the lower mobility of the side Ts groups and hence lower integral values in the spectrum. The reaction of Dex-Ts with EA was documented by nitrogen analysis; 5.04 wt.% nitrogen in Dex-EA indicated that ~80% of the glucose units were modified by EA. Finally, after the reactions of Dex-EA with  $\beta$ -CD-VS and Dex- $\beta$ -CD with VDPA, 1.40 wt.% sulfur and 6.62 wt.% phosphorus were found in the DPA-Dex- $\beta$ -CD polymer, respectively (Table S1). This suggests that ~70% of the glucose units in Dex were modified by  $\beta$ -CD, which is comparable to the  $^{13}\text{C}$  NMR results.

### 3.3. Preparation of Silver-Sulfamethazine-Conjugated $\beta$ -Cyclodextrin/Dextran-Coated IONs (ION@DPA-Dex- $\beta$ -CD-SMT-Ag)

SMT-Ag was selected as an antibacterial agent in this report, as it has a substantially higher minimal inhibitory concentration than SMT alone. In order to prepare IONs conjugated with the SMT-Ag antibiotic as an efficient drug delivery platform, IONs were coated with DPA-Dex- $\beta$ -CD to form ION@DPA-Dex- $\beta$ -CD particles (Figure 3). As the organic coating was not contrasted in the TEM, the number-average diameter and dispersity of ION@DPA-Dex- $\beta$ -CD did not differ from neat IONs (Table 1). In contrast, the hydrodynamic diameter slightly increased ( $D_h = 155 \pm 2$  nm) due to the presence of the DPA-Dex- $\beta$ -CD layer on the particle surface. At the same time, the small polydispersity ( $PD = 0.07$ ) indicated a narrow distribution of particle sizes. In addition, the absolute value of  $\xi$ -potential of ION@DPA-Dex- $\beta$ -CD particles decreased from  $-26 \pm 5$  mV for neat IONs to  $-18 \pm 4$  mV due to the shielding of the DPA-Dex- $\beta$ -CD shell. The advantage of diphosphonic acid in the DPA-Dex- $\beta$ -CD conjugate consisted in its ability to complex with Fe ions of IONs to form stable water-dispersible particles [40]. Mixing the ION@DPA-Dex- $\beta$ -CD particles with SMT-Ag then resulted in its complexation with  $\beta$ -CD to form ION@DPA-Dex- $\beta$ -CD-SMT-Ag particles (Figure 3). While their  $D_n$  were almost the same as that of the ION@DPA-Dex- $\beta$ -CD particles, the  $D_h$  increased to  $244 \pm 3$  nm ( $PD = 0.29$ ) and the  $\xi$ -potential decreased to  $-36 \pm 2$  mV, probably due to the adsorption of hydroxyl ions originating from  $\text{NH}_4\text{OH}$ .

**Table 1.** Physicochemical characterization of particles.

	$D_n$ (nm)	$D$	$D_h$ (nm)	$PD$	$\zeta$ -Potential (mV)	Coating (wt.%)
IONs	$8 \pm 2$	1.29	$108 \pm 1$	0.13	$-26 \pm 5$	-
ION@DPA-Dex- $\beta$ -CD	$9 \pm 2$	1.28	$155 \pm 2$	0.07	$-18 \pm 4$	10.8
ION@DPA-Dex- $\beta$ -CD-SMT-Ag	$8 \pm 2$	1.26	$244 \pm 3$	0.29	$-36 \pm 2$	13.1

$D_n$ —number-average diameter (TEM),  $D$ —dispersity (TEM),  $D_h$ —hydrodynamic diameter (DLS),  $PD$ —polydispersity (DLS).

The surface composition of ION@DPA-Dex- $\beta$ -CD and ION@DPA-Dex- $\beta$ -CD-SMT-Ag was further analyzed by FTIR spectroscopy (Figure 4c). The bands at 1025 and 1358  $\text{cm}^{-1}$  were attributed to  $\nu_{\text{as}}(\text{C-O-C})$  asymmetric and  $\nu_{\text{s}}(\text{CH}_2)$  symmetric stretching vibration, respectively, confirming the presence of DPA-Dex- $\beta$ -CD on the ION surface. The new peaks at 860, 1243, 1418 and 1580  $\text{cm}^{-1}$  in the spectrum of ION@DPA-Dex- $\beta$ -CD-SMT-Ag were assigned to  $\nu(\text{C-H}_{\text{ar}})$ ,  $\nu(\text{C-N})$ ,  $\delta(\text{C-H}_{\text{ar}})$  and  $\nu(\text{C=C})$  vibrations, respectively. These bands were similar to those in the spectrum of SMT-Ag, confirming its incorporation in ION@DPA-Dex- $\beta$ -CD-SMT-Ag particles. The content of the DPA-modified polysaccharide on the particle surface was then analyzed by TGA (Figure 4d). In the thermograms of ION@DPA-Dex- $\beta$ -CD and ION@DPA-Dex- $\beta$ -CD-SMT-Ag, the initial weight loss below 120  $^\circ\text{C}$  was due to the dehydration of the particles. Losses above 120  $^\circ\text{C}$  were attributed to the decomposition of the organic shell on the particles surface. As a result, the amount

of coating on the ION@DPA-Dex- $\beta$ -CD and ION@DPA-Dex- $\beta$ -CD-SMT-Ag particles was 10.8 and 13.1 wt.%, respectively (Table 1). The 2.3% increase in organic content in the ION@DPA-Dex- $\beta$ -CD-SMT-Ag nanoparticles was due to the incorporation of SMT-Ag (Figure 4d). The antibiotic content in the particles was calculated to be  $\sim 29$   $\mu\text{g}$  per mg due to the fact that the silver in SMT-Ag is non-flammable.

SMT-Ag is highly hydrophobic, with water solubility  $< 3$   $\mu\text{g}/\text{mL}$ , as determined by UV-Vis spectrophotometry, which makes the binding of SMT-Ag to the carrier by adsorption or complexation quite challenging. However, some silver sulfonamides show increased solubility in ammonia [41]. The solubility of STM-Ag in 0.06% ammonia was nine times higher than that in water, reaching  $18 \pm 0.2$   $\mu\text{g}/\text{mL}$ , which may potentially simplify drug loading. In addition,  $\beta$ -CD forms a complex with sulfamethazine, which promotes its solubility in water [19]. Thus, after the addition of  $\beta$ -CD, the solubility of SMT-Ag increased twice, reaching  $38 \pm 0.4$   $\mu\text{g}/\text{mL}$ , probably due to the formation of an inclusion complex of  $\beta$ -CD with SMT-Ag. All these indicate that  $\beta$ -CD-containing carriers based on IONs are able to encapsulate SMT-Ag. The amount of SMT-Ag incorporated in the particles was  $24 \pm 0.6$   $\mu\text{g}$  of SMT-Ag per mg, which was comparable to the TGA results (Table 2). It should be added that various organic molecules, including SMT-Ag, can adsorb on the surface of IONs due to the large and charged surface area. According to UV-Vis spectroscopy,  $3 \pm 0.2$   $\mu\text{g}$  SMT-Ag per mg was adsorbed on neat IONs, from which  $LE = 0.3\%$  SMT-Ag was calculated (Equation (1)). In contrast, the  $LE$  of ION@DPA-Dex- $\beta$ -CD-SMT-Ag particles was 2.1% (Table 2), indicating that the Dex- $\beta$ -CD shell increased the  $LE$  for ION@DPA-Dex- $\beta$ -CD-SMT-Ag seven times compared with neat particles. In contrast to other drug delivery carriers, such as hollow porous silica particles ( $LE > 9\%$ ) or magnetic core-shell  $\text{Mn}_{0.3}\text{Fe}_{2.7}\text{O}_4@SiO_2$  nanoparticles ( $LE = 10.4\%$ ), the ION@DPA-Dex- $\beta$ -CD-SMT-Ag particles had lower drug loading [42,43]. However, the loading efficiency depends on the properties of both the carrier and the drug, such as molecular weight, particle volume and surface area, affinity of the drug to the carrier, etc. [44]. While the ION@DPA-Dex- $\beta$ -CD particles could adsorb the drug only on the surface and in the polymer corona, the silica particles could utilize the entire volume of the inner cavities and surface for loading. It should also be taken into account that low antibiotic content does not necessarily mean low antibacterial efficacy. For example, the nanofibers loaded with 2  $\mu\text{g}$  of silver-sulfadiazine per mg showed high antibacterial activity against *E. coli* and *Acinetobacter baumannii* [45].

**Table 2.** Silver-sulfamethazine (SMT-Ag) loading efficiency ( $LE$ ) of IONs and ION@DPA-Dex- $\beta$ -CD particles.

	SMT-Ag Content ( $\mu\text{g}/\text{mg}$ of IONs)	$LE$ (%)
IONs	$3 \pm 0.2$	$0.3 \pm 0.02$
ION@DPA-Dex- $\beta$ -CD	$24 \pm 0.6$	$2.1 \pm 0.03$

### 3.4. Antimicrobial Effects

#### 3.4.1. Qualitative DDT Evaluation

Sulfamethazine is a traditional antibiotic used to treat Gram-positive bacterial infections, including staphylococcal infections (respiratory tract, urinary tract, etc.) in humans and animals. DDT is a standardized method recommended by norm-making authorities (e.g., EUCAST, CLSI and AOAC) to evaluate the antimicrobial effects of compounds, including pharmaceuticals and disinfectants. In these trials, a screening phase is commonly performed to study newly synthesized or naturally isolated molecules for use as antimicrobials. EUCAST-based methods depend on microbial physiology, as the tested microorganisms should have reached their optimum physiological fitness at the time of DDT evaluation. Therefore, the inhibition zones for bacteria (*S. aureus* and *E. coli*) were assessed within a growth span of 24 h; the same applied to the yeast *C. albicans*, while mold (*A. niger*) needed 72 h to develop mature hyphal growth. The aim was to select the most

promising molecules to be submitted for further, more accurate but also more laborious and costly subsequent quantitative tests, such as minimum inhibitory concentration (MIC) and minimum microbicidal concentration (MMC), as well as toxicity tests, etc. Our DDT results showed only limited activity of the ION@DPA-Dex- $\beta$ -CD-SMT-Ag particles against *S. aureus*, as well as against Gram-negative *E. coli* and even against the mold *A. niger*, as only fine zones with a radius of ~1–2 mm were present around the discs. The DDT method uses the free diffusion of the antimicrobial agent into the cultivation medium, and, since the tested particle dispersions were colloidal in nature, diffusion of their active ingredient was thus obviously limited (Table 3). This statement was also indirectly demonstrated in a complementary experiment with a free SMT solution in the presence of particles. This solution provided an inhibition zone around the discs due to the diffusion effect; particle dispersion with free SMT showed activity against *S. aureus* with inhibition zone diameters of 5.4 and 10.2 mm for 40 and 120  $\mu\text{g}$  of particles per 5- and 10-mm disc, respectively. In contrast, neat IONs and ION@DPA-Dex- $\beta$ -CD particles did not show antimicrobial activity. Thus, the observed effect of the microbial growth inhibition effect was clearly related to the active compound (SMT-Ag) encapsulated in the tested particles.

**Table 3.** Qualitative and quantitative evaluation of antimicrobial activity of nanoparticles.

Microorganism	Test	<i>Staphylococcus aureus</i> CCM 2022		<i>Escherichia coli</i> CCM 3954		<i>Candida albicans</i> CCM 8186		<i>Aspergillus niger</i>	
		DDT	MIC/MBC ( $\mu\text{g}/\text{mL}$ )	DDT	MIC/MBC ( $\mu\text{g}/\text{mL}$ )	DDT	MIC/MMC ( $\mu\text{g}/\text{mL}$ )	DDT	MIC/MMC ( $\mu\text{g}/\text{mL}$ )
IONs		Growth around the disc/NT	NE/NE	Growth around the disc/NT	NT	Growth around the disc/growth within the drop	NT	Growth around the disc/NT	NT
ION@DPA-Dex- $\beta$ -CD		Growth around the disc/NT	NE/NE	Growth around the disc/NT	NT	Growth around the disc/growth within the drop	NT	Growth around the disc/NT	NT
ION@DPA-Dex- $\beta$ -CD-SMT-Ag		2 mm inhibition zone/no growth within the drop	500/NE	1 mm inhibition zone/no growth within the drop	500/1000	Growth around the disc/growth within the drop	250/NE	2 mm inhibition zone/no growth within the drop	250/1000

DDT—disc diffusion test (40  $\mu\text{g}$  of particles, i.e., 10  $\mu\text{L}$  drop on 5 mm disc); MIC/MBC/MMC—minimum inhibitory, bactericidal and microbicidal concentrations; NT – not tested; NE – not effective within the tested range of concentration (2.5–1500  $\mu\text{g}/\text{mL}$ ).

### 3.4.2. Quantitative MIC/MBC/MMC Evaluation

Since DDT provided only a qualitative assessment of antibacterial activity, the MIC/MBC/MMC assay was selected to quantify the effect. The MIC parameter is a basic quantitative descriptor of the antimicrobial potential of compounds, indicating their lowest concentration that inhibits the growth of a specific microbe under standard test conditions according to the analytical authority (e.g., EUCAST). In any case, the value itself does not describe whether the antimicrobial effect is static—only postponing microbial growth due to reversible changes in the microbial cell—or cidal, i.e., the microbial cells are devitalized completely. It is the microbial devitalization potential that characterizes the MBC/MMC parameter. While the ION@DPA-Dex- $\beta$ -CD-SMT-Ag particles showed good antibacterial effect against *S. aureus* and *E. coli* according to the MIC/MBC test, the antifungal activity against *C. albicans* and *A. niger* was even more pronounced (Figure 5).

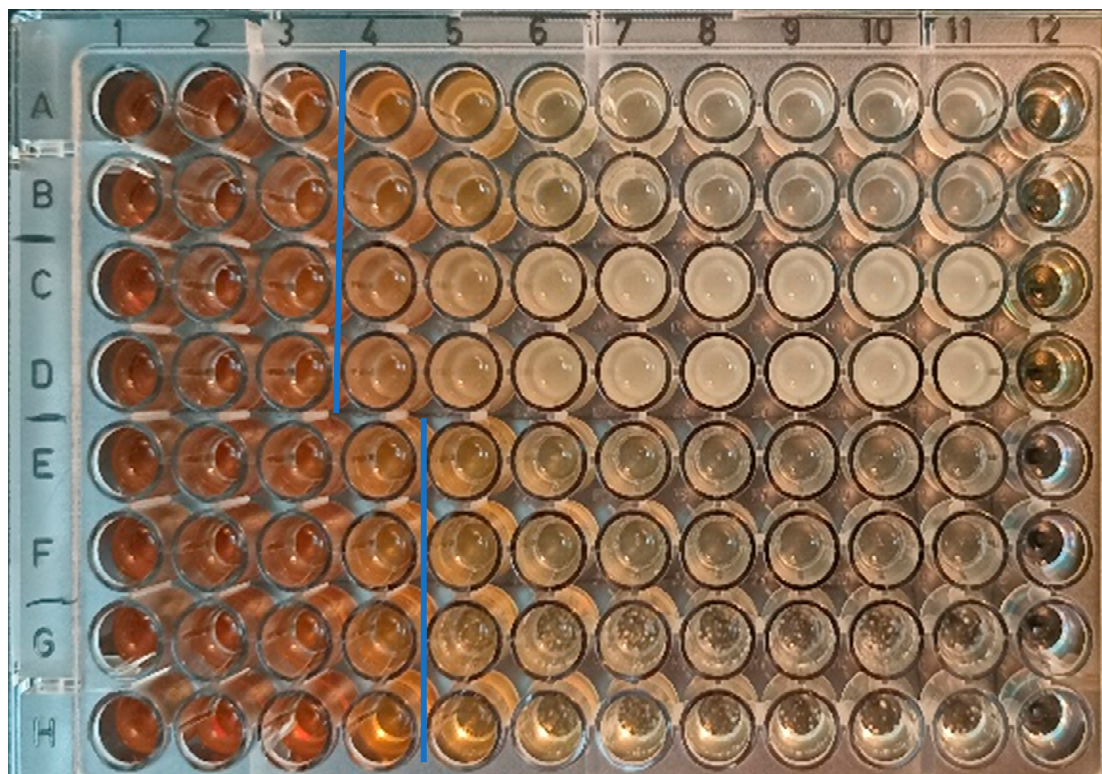


**Figure 5.** MIC of ION-DEX-CD-SMT-Ag; columns 1–10, concentration 1500–2.5 µg/mL; column 11, positive control; column 12, negative control. Row A, B—*S. aureus*; row C, D—*E. coli*; row E, F—*C. albicans*; row G, H—*A. niger*. The blue lines show the boundary between no growth and pathogen growth; column 3/4 is for rows A–D, and column 4/5 is for rows E–H.

This enhanced antibacterial efficiency can be advantageously used, for example, on medical tools and devices to prevent the formation of *C. albicans* biofilms, which account for the largest proportion of hospital-acquired fungal infections. For ION@DPA-Dex-β-CD-SMT-Ag particles, the lowest concentration of the antimicrobial agent, which visibly inhibited the growth of the microorganism, was quite high (500/1000 µg/mL; Table 3). Note that the above values refer to ION@DPA-Dex-β-CD-SMT-Ag particles. After recalculation, this means that the MIC/MBC for SMT-Ag was 12/24 µg/mL, which represents a higher antimicrobial activity than in previously published work [4]. In the agro-food sector, Ag nanoparticles (6–12 nm) are typically used at a concentration of 400 mg/L, which shows high antibacterial efficacy [46]; however, according to other sources, concentrations as low as 4–16 mg/L have been found to be sufficiently effective [47]. In the case of antifungal activity, MIC/MMC was at the level of 250/1000 µg/mL (Table 3). Thus, the antimicrobial effect of Ag in the particles is most likely responsible for this antifungal activity, while the antibacterial activity may be related to the presence of SMT, especially against *S. aureus*, although, as expected, no additive effect of combined SMT-Ag action was observed. This observation may be related to the steric effect of the particles. Since eukaryotic fungal cells are larger than bacteria and because both *C. albicans* and *A. niger* form hyphal structures, their surface exposed to biocide-conjugated particles is also much larger. The mechanism of the antimicrobial effect of Ag is to break down the microbial cell wall structure, allowing ions (or other agents bound to the particles) to penetrate into the cells [48]. Although the repair mechanisms of cell damage due to antimicrobial agents are more complex in eukaryotes than in prokaryotic bacteria, with rapid penetration of the toxic substances into the cells, the toxic effect can occur even at low concentrations.

#### 4. Conclusions

In this report, we developed an original multistep procedure for the preparation of a magnetically controlled drug delivery system. Due to their magnetic nature and non-toxicity, IONs were used as carrier particles. Dex modified with  $\beta$ -CD was selected as the ION coating because both substances are biocompatible and do not cause nonspecific sorption of proteins in the bloodstream. In addition, Dex provides good stabilization of the nanoparticle dispersion, while  $\beta$ -CD can easily capture the SMT-Ag antibiotic for future delivery to the target site due to the presence of an internal hydrophobic pocket. In this way, highly hydrophobic antibiotics such as SMT-Ag can be solubilized, which is essential for their effective functioning in the affected tissue of the organism; this also extends the range of applicability of hydrophobic drugs. The synthetic procedure involved the reaction of  $\beta$ -CD-Ts with EA, resulting in  $\beta$ -CD-EA with a secondary amino group, which required a large molar excess of EA relative to  $\beta$ -CD to achieve a reasonable yield. The amino group of  $\beta$ -CD-EA then reacted with DVS to yield vinyl sulfone-functionalized  $\beta$ -cyclodextrin ( $\beta$ -CD-VS), which combined the ability of  $\beta$ -CD to carry SMT-Ag antibiotic with the good reactivity of the vinyl sulfone group towards Dex-EA. This highly efficient reaction produced Dex- $\beta$ -CD, in which  $\sim 70\%$  of the glucose units reacted with  $\beta$ -CD. The resulting Dex- $\beta$ -CD conjugate then reacted with VDPA-containing diphosphonate groups, which complexed well with the surface Fe ions of the IONs to form DPA-Dex- $\beta$ -CD-coated magnetic nanoparticles. Finally, SMT-Ag was successfully incorporated into  $\beta$ -CD in ION@DPA-Dex- $\beta$ -CD particles; the antibiotic content was 24  $\mu\text{g}$  per mg. The obtained ION@DPA-Dex- $\beta$ -CD-SMT-Ag nanoparticles were colloidal stable in water due to the high absolute value of  $\xi$ -potential ( $-36$  mV). To the best of our knowledge, there are currently no papers addressing the development of such magnetic iron oxide-based carriers for targeted delivery of silver-sulfamethazine. In addition, the magnetic core of the newly developed ION@DPA-Dex- $\beta$ -CD-SMT-Ag drug delivery system can be used as a contrast agent for magnetic resonance imaging, which will allow monitoring of inflammation treatment at the cellular level.

Antibacterial in vitro tests showed that the ION@DPA-Dex- $\beta$ -CD-SMT-Ag nanoparticles exhibited bactericidal activity against Gram-positive *S. aureus* and Gram-negative *E. coli* bacteria (MIC/MBC = 500/1000  $\mu\text{g}/\text{mL}$ ). At the same time, the antifungal activity against *C. albicans* and *A. niger* was even more pronounced, with MIC/MMC of ION@DPA-Dex- $\beta$ -CD-SMT-Ag particles reaching 250/1000  $\mu\text{g}/\text{mL}$ . Targeted administration of antibiotics can thus overcome some of the shortcomings of systemic therapy, such as low concentrations at the site of the inflammation and antibiotic accumulation at the unwanted site. The magnetic nature of the ION@DPA-Dex- $\beta$ -CD-SMT-Ag nanoparticles responding to an external magnetic field is particularly important, as magnetic targeting can increase the local concentration of the antibiotic at the affected site and thus the antimicrobial effect. Magnetically controlled ION@DPA-Dex- $\beta$ -CD-SMT-Ag nanoparticles could be thus promising for the topical delivery of antimicrobials to treat bacterial or fungal infections in animals and eventually in humans; nevertheless, future research is needed to further clarify the antimicrobial mechanism.

**Supplementary Materials:** The following supporting information can be downloaded at: <https://www.mdpi.com/article/10.3390/nano14040371/s1>. Table S1: Nitrogen, sulfur and phosphorus content in Dex and  $\beta$ -CD derivatives. Figure S1:  $^1\text{H}$  NMR spectra of 4-toluenesulfonic acid (TsOH), 4-toluenesulfonyl chloride (TsCl) and 4-toluenesulfonic anhydride (Ts<sub>2</sub>O) in DMSO-d<sub>6</sub> at 25 °C. Figure S2:  $^1\text{H}$  NMR spectra of (a)  $\beta$ -cyclodextrin and (b)  $\beta$ -cyclodextrin modified with tosyl groups dissolved in DMSO-d<sub>6</sub>, (c)  $^1\text{H}$ - $^1\text{H}$  2D NOESY NMR and (d) 2D DOSY NMR spectra of tosyl-modified  $\beta$ -CD. Figure S3: (a,b)  $^1\text{H}$  NMR and (c,d) DOSY NMR spectra of (a,c)  $\beta$ -CD-EA and (b,d)  $\beta$ -CD-VS. Figure S4:  $^1\text{H}$  NMR spectra of (a) Dex-Ts and (b) Dex-EA. Figure S5: (a)  $^1\text{H}$  NMR spectrum of DPA-Dex- $\beta$ -CD and (b)  $^{13}\text{C}$  NMR spectrum of DPA-Dex- $\beta$ -CD. Figure S6:  $^{13}\text{C}$  NMR spectra (90–110 ppm region) of (a) Dex-EA, (b)  $\beta$ -CD-EA and (c) DPA-Dex- $\beta$ -CD. Figure S7:  $^{31}\text{P}$  NMR spectrum of DPA-Dex- $\beta$ -CD. Figure S8:  $^{13}\text{C}$  NMR spectrum of Dex-EA. Figure S9:  $^{13}\text{C}$  NMR spectrum of CD-EA.

**Author Contributions:** Investigation and Writing—Original Draft Preparation, A.B.S.; Conceptualization, V.P.; Methodology, H.M.; Formal Analysis, A.M. and R.L.; Investigation and Data Curation, E.P.; Writing – Review, Editing and Supervision, D.H. All authors have read and agreed to the published version of the manuscript.

**Funding:** The authors acknowledge the support of the National Institute for Cancer Research (Programme EXCELES; No. LX22NPO5102), funded by the European Union—Next Generation EU and Cedars-Sinai Medical Center’s International Research and Innovation in Medicine Program and the RECOOP HST Association.

**Data Availability Statement:** The data presented in this study are available on request from the first author.

**Conflicts of Interest:** The authors declare no conflict of interest.

## References

1. Aslam, B.; Wang, W.; Arshad, M.I.; Khurshid, M.; Muzammil, S.; Rasool, M.H.; Nisar, M.A.; Alvi, R.F.; Aslam, M.A.; Qamar, M.U.; et al. Antibiotic resistance: A rundown of a global crisis. *Infect. Drug Resist.* **2018**, *11*, 1645–1658. [\[CrossRef\]](#)
2. Oung, A.; Bhattacharyya, J. Sulfonamide drugs: Structure, antibacterial property, toxicity, and biophysical interactions. *Biophys. Rev.* **2021**, *13*, 259–272. [\[CrossRef\]](#)
3. Niu, Z.; Liu, Y.; Li, X.; Zhu, H.; Zhang, M.; Yan, K.; Chen, H. Colorimetric detection of sulfamethazine based on target resolved calixarene derivative stabilized gold nanoparticles aggregation. *Microchim. Acta* **2022**, *189*, 71. [\[CrossRef\]](#)
4. Tailor, S.M.; Patel, U.H. Synthesis, spectroscopic characterization, antimicrobial activity and crystal structure of silver and copper complexes of sulfamethazine. *J. Coord. Chem.* **2015**, *68*, 2192–2207. [\[CrossRef\]](#)
5. Eleraky, N.E.; Allam, A.; Hassan, S.B.; Omar, M.M. Nanomedicine fight against antibacterial resistance: An overview of the recent pharmaceutical innovations. *Pharmaceutics* **2020**, *12*, 142. [\[CrossRef\]](#)
6. Wahajuddin; Arora, S. Superparamagnetic iron oxide nanoparticles: Magnetic nanoplatforms as drug carriers. *Int. J. Nanomed.* **2012**, *7*, 3445–3471. [\[CrossRef\]](#)
7. Chang, Y.-L.; Liao, P.-B.; Wu, P.-H.; Chang, W.-J.; Lee, S.-Y.; Huang, W.-M. Cancer cytotoxicity of a hybrid hyaluronan-superparamagnetic iron oxide nanoparticle material: An *in-vitro* evaluation. *Nanomaterials* **2022**, *12*, 496. [\[CrossRef\]](#)
8. Mylkie, K.; Nowak, P.; Rybczynski, P.; Ziegler-Borowska, M. Polymer-coated magnetite nanoparticles for protein immobilization. *Materials* **2021**, *14*, 248. [\[CrossRef\]](#)
9. Tassa, C.; Shaw, S.Y.; Weissleder, R. Dextran-coated iron oxide nanoparticles: A versatile platform for targeted molecular imaging, molecular diagnostics, and therapy. *Acc. Chem. Res.* **2011**, *18*, 842–852. [\[CrossRef\]](#)
10. Lemechko, P.; Renard, E.; Guezennec, J.; Guezennec, C.; Langlois, V. Synthesis of dextran-graft-PHBHV amphiphilic copolymer using click chemistry approach. *Reac. Funct. Polym.* **2012**, *72*, 487–494. [\[CrossRef\]](#)
11. Yang, J.; Liu, Y.; Wang, H.; Liu, L.; Wang, W.; Wang, C.; Wang, Q.; Liu, W. The biocompatibility of fatty acid modified dextran-aggmatine bioconjugate gene delivery vector. *Biomaterials* **2012**, *33*, 604–613. [\[CrossRef\]](#)
12. Heinze, T.; Michealis, N.; Hornig, S. Reactive polymeric nanoparticles based on unconventional dextran derivatives. *Eur. Polym. J.* **2007**, *43*, 697–703. [\[CrossRef\]](#)
13. Xu, J.; Tian, Y.; Li, Z.; Tan, B.H.; Tang, K.Y.; Tam, K.C.  $\beta$ -Cyclodextrin functionalized magnetic nanoparticles for the removal of pharmaceutical residues in drinking water. *J. Ind. Eng. Chem.* **2022**, *109*, 461–474. [\[CrossRef\]](#)
14. Ahmed, G.H.G.; Laño, R.B.; Calzón, J.A.G.; García, M.E.D. Magnetic nanoparticles grafted with  $\beta$ -cyclodextrin for solid-phase extraction of 5-hydroxy-3-indole acetic acid. *Microchim Acta* **2014**, *181*, 941–948. [\[CrossRef\]](#)
15. Banerjee, S.S.; Chen, D.-H. Magnetic nanoparticles grafted with cyclodextrin for hydrophobic drug delivery. *Chem. Mater.* **2007**, *19*, 6345–6349. [\[CrossRef\]](#)
16. Tang, X.; Wen, Y.; Zhang, Z.; Zhu, J.; Song, X.; Li, J. Rationally designed multifunctional nanoparticles as GSH-responsive anticancer drug delivery systems based on host-guest polymers derived from dextran and  $\beta$ -cyclodextrin. *Carbohydrate Polym.* **2023**, *320*, 121207. [\[CrossRef\]](#)
17. Zhang, Y.; Jiang, F.; Huang, D.; Hou, S.; Wang, H.; Wang, M.; Chi, Y.; Zhao, Z. A facile route to magnetic mesoporous core-shell structured silicas containing covalently bound cyclodextrins for the removal of the antibiotic doxycycline from water. *RSC Adv.* **2018**, *8*, 31348–31357. [\[CrossRef\]](#)
18. Zhang, Y.; Li, J.; Wang, F.F.; Wu, G.; Qv, X.; Hong, H.; Liu, C. Recovery and separation of erythromycin from industrial wastewater by imprinted magnetic nanoparticles that exploit  $\beta$ -cyclodextrin as the functional monomer. *J. Sep. Sci.* **2016**, *39*, 450–459. [\[CrossRef\]](#)
19. Zoppi, A.; Delrivo, A.; Aiassa, V.; Longhi, M.R. Binding of sulfamethazine to  $\beta$ -cyclodextrin and methyl- $\beta$ -cyclodextrin. *AAPS PharmSciTech* **2013**, *14*, 727–735. [\[CrossRef\]](#)
20. Abou-El-Sherbini, K.S.; Amer, M.H.A.; Abdel-Aziz, M.S.; Hamzawy, E.M.A.; Sharmoukh, W.; Elnagar, M.M. Encapsulation of biosynthesized nanosilver in silica composites for sustainable antimicrobial functionality. *Glob. Chall.* **2018**, *2*, 1800048. [\[CrossRef\]](#)
21. Wang, Q.; Zhang, Y.; Li, Q.; Chen, L.; Liu, H.; Ding, M.; Dong, H.; Mou, Y. Therapeutic applications of antimicrobial silver-based biomaterials in dentistry. *Int. J. Nanomed.* **2022**, *17*, 443–462. [\[CrossRef\]](#)

22. Zhang, J.; Xu, Q.; Li, H.; Zhang, S.; Hong, A.; Jiang, Y.; Hu, N.; Chen, G.; Fu, H.; Yuan, M.; et al. Self-powered electrodeposition system for sub-10-nm silver nanoparticles with high-efficiency antibacterial activity. *J. Phys. Chem. Lett.* **2022**, *13*, 6721–6730. [CrossRef]
23. Degenhardt, C.R.; Burdsall, D.C. Synthesis of ethenylidenebis(phosphonic acid) and its tetraalkyl esters. *J. Org. Chem.* **1986**, *51*, 3488–3490. [CrossRef]
24. Zhong, N.; Byun, H.-S.; Bittman, R. An improved synthesis of 6-O-monotosyl-6-deoxy- $\beta$ -cyclodextrin. *Tetrahedron Lett.* **1998**, *39*, 2919–2920. [CrossRef]
25. del Castillo, T.; Marales-Sanfrutos, J.; Santoyo-González, F.; Magez, S.; Lopez-Jaramillo, F.J.; Garcia-Salcedo, J.A. Monovinyl sulfone  $\beta$ -cyclodextrin. A flexible drug carrier system. *ChemMedChem* **2014**, *9*, 383–389. [CrossRef]
26. Zasońska, B.A.; Boiko, N.; Klyuchivska, O.; Trchová, M.; Petrovský, E.; Stoika, R.; Horák, D. Silica-coated  $\gamma$ -Fe<sub>2</sub>O<sub>3</sub> nanoparticles: Preparation and engulfment by mammalian macrophages. *J. Nanopharm. Drug Deliv.* **2013**, *1*, 182–192. [CrossRef]
27. Stejskal, E.O.; Tanner, J.E. Spin diffusion measurements: Spin echoes in the presence of a time-dependent field gradient. *J. Chem. Phys.* **1965**, *42*, 288–292. [CrossRef]
28. EUCAST Disk Diffusion Method for Antimicrobial Susceptibility Testing, Version 11.0. Available online: [www.eucast.org/fileadmin/src/media/PDFs/EUCAST\\_files/Disk\\_test\\_documents/2023\\_manuals/Manual\\_v\\_11.0\\_EUCAST\\_Disk\\_Test\\_2023.pdf](http://www.eucast.org/fileadmin/src/media/PDFs/EUCAST_files/Disk_test_documents/2023_manuals/Manual_v_11.0_EUCAST_Disk_Test_2023.pdf) (accessed on 1 January 2023).
29. Nweze, E.I.; Mukherjee, P.K.; Ghannoum, M.A. Agar-based disk diffusion assay for susceptibility testing of dermatophytes. *J. Clin. Microbiol.* **2010**, *48*, 3750–3752. [CrossRef]
30. Laurent, S.; Forge, D.; Port, M.; Roch, A.; Robic, C.; Vander Elst, L.; Muller, R.N. Magnetic iron oxide nanoparticles: Synthesis, stabilization, vectorization, physicochemical characterizations, and biological applications. *Chem. Rev.* **2008**, *108*, 2064–2110. [CrossRef]
31. Zasońska, B.A.; Bober, P.; Jošt, P.; Petrovský, E.; Boštík, P.; Horák, D. Magnetoconductive maghemite core/polyaniline shell nanoparticles as promising tools for biomedical applications. *Colloids Surf. B* **2016**, *141*, 382–389. [CrossRef]
32. Winkler, R.; Ciria, M.; Ahmad, M.; Plank, H.; Marcuello, C. A review of the current state of magnetic force microscopy to unravel the magnetic properties of nanomaterials applied in biological systems and future directions for quantum technologies. *Nanomaterials* **2023**, *13*, 2585. [CrossRef]
33. Babič, M.; Horák, D.; Jendelová, P.; Glogarová, K.; Herynek, V.; Trchová, M.; Likavčanová, K.; Hájek, M.; Syková, E. Poly(*N,N*-dimethylacrylamide)-coated maghemite nanoparticles for stem cell labeling. *Bioconjugate Chem.* **2009**, *20*, 283–294. [CrossRef]
34. Carone, A.; Emilsson, S.; Mariani, P.; Désert, A.; Parola, S. Gold nanoparticle shape dependence of colloidal stability domains. *Nanoscale Adv.* **2023**, *5*, 2017–2026. [CrossRef]
35. Hu, Q.; Lu, Y.; Luo, Y. Recent advances in dextran-based drug delivery systems: From fabrication strategies to applications. *Carbohydr. Polym.* **2021**, *264*, 117999. [CrossRef]
36. Schneider, H.J.; Hacket, F.; Rüdiger, V.; Ikeda, H. NMR studies of cyclodextrins and cyclodextrin complexes. *Chem. Rev.* **1998**, *98*, 1755–1785. [CrossRef]
37. Purama, R.K.; Goswami, P.; Khan, A.T.; Goyal, A. Structural analysis and properties of dextran produced by *Leuconostoc mesenteroides* NRRL B-640. *Carbohydr. Polym.* **2009**, *76*, 30–35. [CrossRef]
38. Kuniaki, F. The infrared spectrum of dimethyl sulfone. *Bull. Chem. Soc. Jpn.* **1959**, *32*, 1374–1376. [CrossRef]
39. Gong, W. A real-time *in-situ* ATR-FITIR spectroscopic study of linear phosphate on titania surfaces. *Int. J. Miner. Process.* **2001**, *63*, 147–165. [CrossRef]
40. Horwitz, E.P.; Gatrone, R.C.; Nash, K.L. Membrane Extraction with Thermodynamically Unstable Diphosphonic Acid Derivatives. US Patent 5,678,242, 1997. Available online: <https://www.osti.gov/biblio/541723> (accessed on 14 October 1997).
41. Sandmann, B.J.; Nesbitt, R.U.; Sandmann, R.A. Characterization of silver sulfadiazine and related compounds. *J. Pharm. Sci.* **1974**, *63*, 948–951. [CrossRef]
42. Guo, L.; Ping, J.; Qin, J.; Yang, M.; Wu, X.; You, M.; You, F.; Peng, H.A. Comprehensive study of drug loading in hollow mesoporous silica nanoparticles: Impacting factors and loading efficiency. *Nanomaterials* **2021**, *11*, 1293. [CrossRef]
43. Wu, T.; Wang, L.; Gong, M.; Lin, Y.; Xu, Y.; Ye, L.; Yu, X.; Liu, J.; Liu, J.; He, S.; et al. Synergistic effects of nanoparticle heating and amoxicillin on *H. pylori* inhibition. *J. Magn. Magn. Mater.* **2019**, *485*, 95–104. [CrossRef]
44. Bohara, R.A.; Thorat, N. (Eds.) *Hybrid Nanostructures for Cancer Theranostics*; Elsevier: Oxford, UK, 2019. [CrossRef]
45. Mutlu-Ağardan, N.B.; Tort, S.; Aydoğduoğlu, Ş.; Kıymacı, M.E. A new insight to silver sulfadiazine antibacterial dressings: Nanoparticle-loaded nanofibers for controlled drug delivery. *AAPS PharmSciTech* **2023**, *24*, 8. [CrossRef]
46. Parzymies, M.; Pudelska, K.; Poniewozik, M. The use of nano-silver for disinfection of *Pennisetum alopecuroides* plant material for tissue culture. *Acta Sci. Pol. Hortorum Cultus* **2019**, *18*, 127–135. [CrossRef]
47. Sarmast, M.K.; Salehi, H.; Khosh-Khui, M. Nano silver treatment is effective in reducing bacterial contaminations of *Araucaria excelsa* R. Br. var. *glauca* explants. *Acta Biol. Hung.* **2011**, *62*, 477–484. [CrossRef] [PubMed]
48. Dibrov, P.; Dzioba, J.; Gosink, K.K.; Häse, C.C. Chemiosmotic mechanism of antimicrobial activity of Ag<sup>+</sup> in *Vibrio cholerae*. *Antimicrob. Agents Chemother.* **2002**, *46*, 2668–2670. [CrossRef] [PubMed]

**Disclaimer/Publisher’s Note:** The statements, opinions and data contained in all publications are solely those of the individual author(s) and contributor(s) and not of MDPI and/or the editor(s). MDPI and/or the editor(s) disclaim responsibility for any injury to people or property resulting from any ideas, methods, instructions or products referred to in the content.